Degradation Estimation and Prediction of Electronic Packages using Data Driven Approach

Prisacaru, Alexandru; Gromala, Przemyslaw Jakub; Han, Bongtae; Zhang, G. Q.

DOI
10.1109/TIE.2021.3068681

Publication date
2021

Document Version
Accepted author manuscript

Published in
IEEE Transactions on Industrial Electronics

Degradation Estimation and Prediction of Electronic Packages using Data Driven Approach

Alexandru Prisacaru, Przemyslaw Gromala, *Member, IEEE*, Bongtae Han, and Guo Qi Zhang, *Life Fellow, IEEE*

***Abstract*—Recent trends in automotive electronics such as automated driving will increase the number and complexity of electronics used in safety relevant applications. Applications in logistics or ridesharing will require a specific year of service rather than the conventional mileage usage. Reliable operations of the electronic systems must be assured at all times, regardless of the usage condition. A more dynamic and on-demand way of assuring the system availability will have to be developed. This paper proposes a thermo-mechanical stress-based prognostics method as a potential solution. The goal is achieved by several novel advancements. On the experimental front, a key microelectronics package is developed to directly apply the prognostics and health management (PHM) concept using a piezoresistive silicon-based stress sensor. Additional hardware for safe and secure data transmission and data-processing is also developed, which is critically required for recording in situ and real-time data. On the data-management front, proper data-driven approaches have to be identified to handle the unique data set from the stress sensor employed in the study. The approaches effectively handle the massive amount of data that reveals the important information and automation of the prognostic process and thus to be able to detect, classify, locate and predict the failure. The statistical techniques for diagnostics and the machine learning (ML) algorithms for health assessment and prognostics are also determined to implement the approaches in a simple, fast but accurate way within the capacity of limited computing power. The proposed prognostics approach is implemented with actual microelectronics packages subjected to harsh accelerated testing conditions. The results corroborate the validity of the proposed prognostics approach.**

***Index Terms*—Piezoresistive Stress Sensor, Data-driven, Electronic Packages, Prognostics and Health Management, Recurrent Neural Network, Machine Learning keywords@ieee.org or visit http://www.ieee.org/documents/taxonomy_v101.pdf.**

I. Introduction

MICROELECTRONICS packages are composed of multi-layer dissimilar materials with complex geometries. These composite interfaces, corners and edges are subjected to various loading conditions during manufacturing as well as operation [1]. The packaging technologies are used to protect sensitive electronic components for various applications such as telecommunication, automotive and aerospace.

During operation, the internal stress state changes, due to the coefficient of thermal expansion (CTE) mismatch among the materials used in the package as well as the stress concentrations at material discontinuities, which can cause thermo-mechanical related failures. According to [2] these failures account for more than 65% of the total failures in electronics.

Prognostics is the process of predicting a future state (of reliability) based on current and historic conditions. Prognostics and health management (PHM) is a method that permits the reliability of a system to be evaluated in its actual life-cycle conditions, to determine the advent of failure, and mitigate the system risks [3]. One of the ways to perform prognostics is to measure the mechanical stresses directly using a stress sensor. Such sensor was developed originally to measure the manufacturing stresses [4], but was extended successfully to various applications including transfer molding [5], packaging [6], molding relaxation [7], prognostics [8] [9] and condition monitoring [10] [11]. In [12] the sensor was packages in a QFN and the stress field has been recorded after the damage. Although, the damage was observed in the stress field the limitation is that the delamination is imposed apriori. Delamination was also reported in [13]. A flip chip as an application was used during the reliability testing. While the delamination was successfully monitored, the delamination happened exactly at the sensor interface and only 11 measuring cells was used.

In the previous related paper [8], delamination was successfully detected in overmolded electronic unit test vehicle using such stress sensor. The propagation of the delamination was also successfully monitored. Yet, the available experimental data was limited (the delamination was apriori imposed), and delamination was correlated with stress data only qualitatively. This is the motivation of the current paper. Algorithms and techniques for automated degradation estimation and prediction for electronic packages using mechanical stress is not yet reported.

Significantly more data are required to predict the health condition quantitatively. They should be collected from multiple samples, and each sample should provide continuous stress signals from the healthy state to the state of complete failure. The previous approach by which the data is handled manually using a degradation model becomes simply unfeasible for such large amount of data [8]. For example, raw data for each sample goes up to 2.5 GB for 2500 Cycles. A Finite Element Method validation of the current experiments used in this paper was performed in [14]. A classical back propagation neural

network was used to estimate the degradation. The results showed that an improved model is needed.

In this paper, the stress-based PHM capability is extended into a quantitative domain where accurate prediction of remaining useful life (RUL) becomes possible. The goal is achieved by several major novel advancements:

- Non-destructive and in-situ detection of the delamination during accelerated testing
- Successful classification of the data obtained from two different failure modes
- Quantitative estimation of delamination location, state of health and degradation of automotive electronic packages using Machine Learning

.

In section II, the general PHM framework adopted in this study is introduced. An experimental setup and a test vehicle are described in Section III. Results from actual tests and various strategies for evaluation and processing the data are presented in Section IV. Diagnostics by means of failure detection, location and classification is shown in Section V. Section VI presents the Health Assessment and Prognostics.

II. Methodology

In this section the PHM framework is presented. The fundamentals of the methods used in the methodology is also discussed. The workflow of the PHM methodology is described in Figure 1.

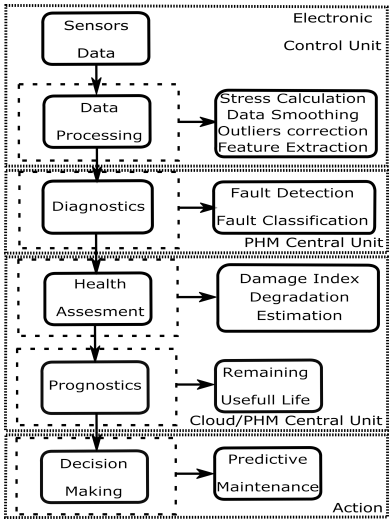

Fig. 1. Algorithm flowchart that depicts the workflow of the PHM methodology and the corresponding hardware.

One of the most important aspects in PHM is the sensor data selection, as it has to be sensitive to a damage of interest. A piezoresistive silicon-based stress sensor was employed in this study, due to its direct connection to any physical changes in the package [15]. The stresses are calculated based on the two measured quantities: (1) the stresses determined from pMOS and nMOS current values and (2) the temperature determined from the voltages. Both pMOS and nMOS (p and n channel MOSFETs) transistors are used for the stress difference $D(\sigma) = \sigma_{XX} - \sigma_{YY}$ calculation and shear stress σ_{XY}, respectively. These values are calculated from the following relationship:

$$D(\sigma) = \sigma_{xx} - \sigma_{yy} = \frac{1}{\pi_{44}^{p}} \frac{I_{OUT} - I_{IN}}{I_{OUT} + I_{IN}} \tag{1}$$

$$\sigma_{xy} = \frac{1}{\pi_{11}^{n} - \pi_{12}^{n}} \frac{I_{OUT} - I_{IN}}{I_{OUT} + I_{IN}} \tag{2}$$

where π_{11}, π_{12},π_{44} are the piezoresistive coefficients of silicon; and I_{IN}, I_{OUT} are the currents measured at the input and output of the sensor, respectively. This data is then passed through a preprocessing step that removes outliers, smoothens the data and extracts the relative stresses caused by the temperature change. More details about the theoretical background of the stress sensor can be found in [16] and the fundamentals of how to use such sensor in reliability are described in detail in [15].

An acquisition unit (AU) is utilized to acquire the sensor signals, and the second unit is to process and transmit the data (PHM Central Unit). Through this platform, the data from the sensors are collected, processed, and transmitted to a cloud or a database server.

A visualization metric is used to observe any change in the sensor data that might indicate a shift from the normal operation. To automate this process, a failure detection algorithm is used in parallel to check if the stress data is within the threshold. Most of the failure detection algorithms can be easily biased by some unknown operating conditions or some other unexpected events. Therefore, a visualization metric is necessary as a robust measure. After the failure is recognized, a diagnostic tool is used to classify the data in groups, which are subsequently assigned to a certain physical quantity. An algorithm for degradation estimation and prediction is then applied to quantitatively assess the failure.

Simple, fast and accurate models are chosen in this methodology. The process of choosing the algorithms is made based on the performance evaluation in comparison with the failure analysis. Scanning Acoustic Microscope (SAM) and cross-sectioning are used collectively for the required detailed failure analysis.

A. Acquisition Unit and Central PHM Unit

As mentioned earlier, the piezoresistive Silicon based stress sensor was developed originally for measuring stresses during the manufacturing processes [17]. A dedicated AU is required to steer the sensor and to successfully record the data. The first AU was developed together with the sensor [18], but its large size and the small number of sensors for simultaneous measurements made it impractical for in-situ applications. The second AU developed by Palczynska [19] made the in-situ measurements possible by scaling down the unit with a 12V power source. In addition, a multiplexer was added to increase the maximum number of sensors. More advancements are required to cope with other challenging issues encountered in actual applications: the large amount of data, further miniaturization, data remote access, computing power, and long running experiments. Such system is depicted in Figure 2.

The newly developed AU consists of Arduino Yun Mini board as well as a custom designed board. The former is used to control and readout the sensor and the latter to power and steer the sensor. The Arduino board is equipped with a μcontroller and a μprocessor that sustains the Wi-Fi shield.

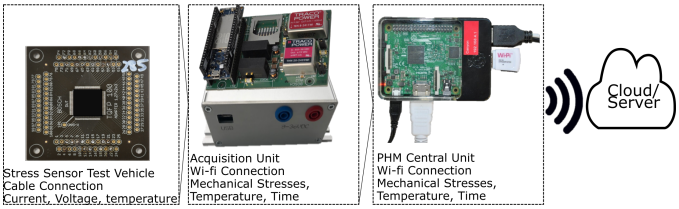

Fig. 2. Data Flow representation. On each chart is described the electronic unit, the connection and the data output.

III. Experimental Setup and Test Vehicle

One critical failure mechanism of semiconductor packages is the loss of adhesion at interfaces causing delamination. Failure modes that are caused by delamination are the passivation damage, wire-bond degradation, intermittent electrical failure, and popcorn cracking.

A. Test Vehicle

The test vehicle (TV) used in this study is a Thin-Quad Flat Package (TQFP) mounted on a Printed Circuit Board (PCB). A TQFP encapsulates eight sensors on a single die, as depicted in Figure 3. Each sensor consists of 60 measurement cells in a 6x10 matrix and every each cell contains the pMOS and nMOS transistor, as shown in Figure 3. Seven TVs fabricated from 2 different molding compounds are used in the experiment. The TVs are numbered as:

MCi_j, where i is the molding compound and j is the sample number.

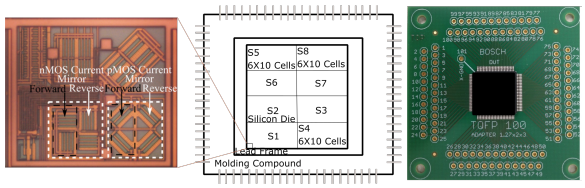

Fig. 3. Test Vehicle. 8 stress sensors encapsulated in a TQFP package mounted on a PCB. It indicates the sensor location, definition and the number of measuring cells.

The TVs use pre-oxidized leadframe, which significantly reduces the interface strength between the molding compound and the copper pad. It is expected that the delamination process starts at different times for $MC1$ and $MC2$.

Temperature shock (TS) testing is used for damage acceleration in the study. A TS equipment used in the experiment contains two separate chambers, which are preset at different temperatures. The temperatures profile consists of $-40°C$ and $150°C$, as shown in Figure 4. Considering the amount of time needed for the AU to acquire one measurement point (MP), every cycle produces two or three measurement points. Several samples are placed on the basket, and the signal wires are taken out though the middle hollow cylinder which is used for the basket movement. The transition between temperatures is short due to the mobility of the basket (according to Figure 4). The stresses inflicted to the samples in this type of chamber are larger than in a regular thermal chamber due to the fast transition. The temperature difference between the test vehicle and the chamber is initially high, imposing extra stresses.

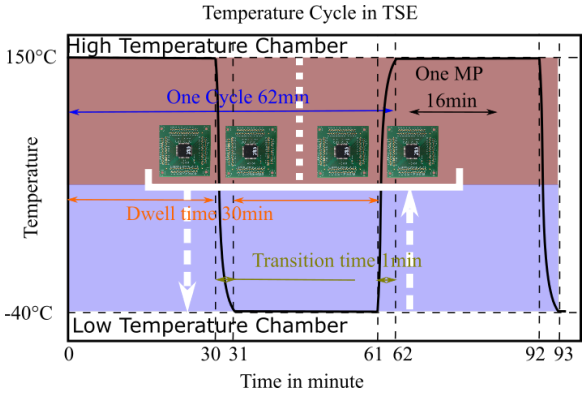

Fig. 4. Temperature cycle duration. Transition time and the dwell time is briefly specified.

IV. Experimental Results

Repeated loading causes accumulated fatigue damage, leading to cracks and rupture. It is generally understood that exposing surface-mount plastic parts to high-temperature reflow profiles can generate package failures if delamination is present. Figure 5 depicts where the delamination occurs and where the stresses are measured in a typical package.

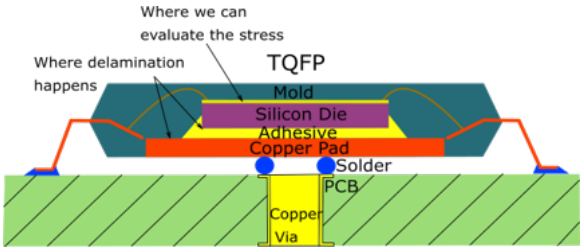

Fig. 5. Package on PCB cross-section. It shows the main elements of the package and illustrates where the stresses are measured. At the same time, where the delamination usually occurs.

Two experiments were performed in two separate TS chambers. The temperature profile used in the experiment is described in Figure 4. In the first experiment, the test vehicles were cycled for 750 TS cycles with 30 minutes dwell time, and in the second experiment, for 1600 TS cycles with 40 minutes dwell time.

The stress data was continuously recorded during TS cycling. The data from the TV stress sensor was captured with the AU by a cable connection, which was placed outside the chamber. The AU was sending the data to the Wi-fi Console, followed by the Raspberry Pi to collect this data from the Console and save it. A simple graphical interface was used in

TABLE I
DATA PROCESSING

Input: Sensors Data $I_{OUT}, I_{IN}, V, Time$
Output: Relative stress difference, Temp, Time per Cycle: $D(\sigma)_{ij} = (\sigma_{xx} - \sigma_{yy})^{ij}_{T=-40°C} - (\sigma_{xx} - \sigma_{yy})^{ij}_{T=150°C}$
1. Stress Difference, temperature and time calculation: DIF_{ik}, TEM_{ik} and TIME_k
2. Data cleaning: Calibration of temperatures and outliers correction: $NAT \in [-1, 1]$, $N/A = 0$
3. Labeling: Temperature classification. $TemCat_k = "high(150°)"\ \forall NAT_k \in [1.00, 0.98]$ $TempCat_k = "low(-40°)"\ \forall NAT_k \in [-0.98, 1.00]$ $TempCat_k = "undefined"\ \forall NAT_k \in [0.98, -0.98]$
4. Smoothing: Sliding Window $DIF_{ik} = \sqrt{\frac{1}{w}\sum_{k=1}^{k=w}(DIF_k - \overline{DIF})^2}$
5. Space Transformation: Cycle space; One value per cycle $(\sigma_{xx} - \sigma_{yy})^{ij} = T_j[(DIF_{ik})]$
$*i = 1, 2, ..., n$ and $n =$ total number of cells
$*j = 1, 2, ..., m$ and $m =$ number of cycles
$*k = 1, 2, ..., p$ and $p =$ total number of measurement points

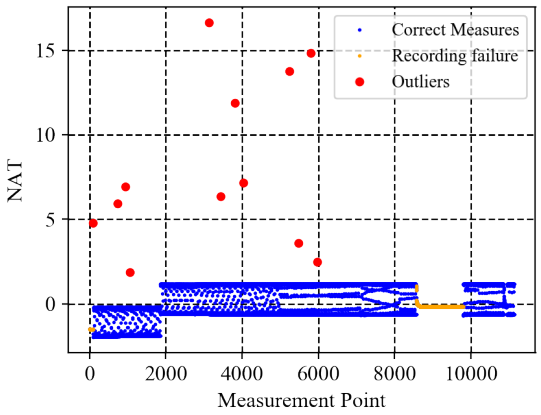

Fig. 6. Normalized average temperature (NAT) of sensor 3. The temperature is calculated at each cell position and then averaged in one value. The jump in the scaling data is represented by a stop and start of the experiment. The orange data is explained by a pause in the chamber operation.

Raspberry Pi to check the status of the experiments and the stresses in real time. At every 50 MPs, the data was sent to the cloud server. The possibility of accessing the Raspberry Pi with a monitor, remote access or a smartphone, provides flexibility and better control over the experiments.

The raw data gathered from the experiment was composed of the high precision physical measures of voltages and currents from each individual cell of the TV and the times when the measurements were performed. By themselves, these measures do not provide any valuable insight into the matter of this study. All this data is contained in a single data set.

A. Data Preprocessing.

The stress difference is computed using equations 1 and 2, with the corresponding currents values from the raw data set. The temperatures are calculated from the measured voltages, and the time for measurements is extracted from raw data. All calculation steps are described in Table I.

Each step is summarized below:

Step 1. DIF stores the stress difference values of each cell per MP, TEM stores the temperature values of each cell per MP and $TIME$ stores the time at the beginning of the recording of each MP. Step 2.Data cleaning techniques usually include detecting N/A values, outliers and gaps on the data. It is always the first step in data preprocessing [20], [21]. These values are shown on Figure 6. Step 3. Handling of outliers on the temperature feature is straightforward as the final distribution along the NAT-axis is known. All values of NAT must fall around +1 and -1 after normalization. Values exceeding these thresholds are data transmission errors and are taken out. Step 4. DIF must pass now through a filtering process to reduce sources of noise [21]. Not all data will be relevant on a later step, so only data points classified as 'high' and 'low' will be filtered for speeding up the process. A window filter of three data points. The value of the data point at the center of the window is replaced by the average of its sides if the standard deviation surpasses a fixed threshold of 1.1. Step 5. After filtering process, 2 or 3 measures on each peak or dwell time of the temperature cycle are kept. A transformation is performed reducing every sequence of MPs to just one point whose value is the average of the original points.

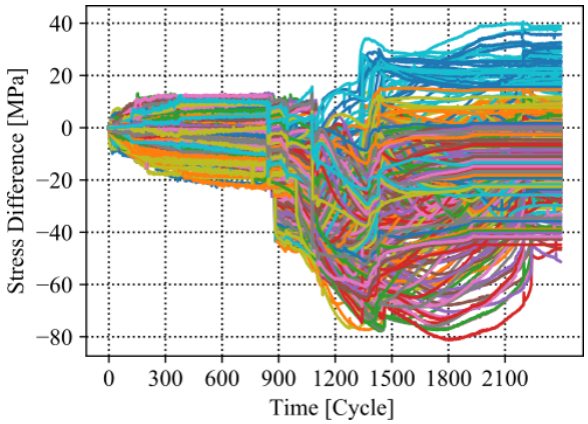

Fig. 7. $MC1\_1$ TV 480 stress difference sensing cells representation during the experiment.

The sensor data set has been reduced finally to an understandable form. The dimensions have been reduced to include one unique signal per cell on the sensor that shows the stress difference variation between the peak low temperature and the peak high temperature of each of the temperature shock cycles the TV was exposed to. Figure 7 depicts such unique signal per cell of all 480 measuring locations. After applying the data processing to the datasets obtained from the experiment the visualization of one single signal per cell is possible, representing the relative values of stresses, by subtracting the residual stresses. These new values are representing the stress given by the temperature change $\Delta T = 190°C$.

B. Visualization Metric

It is reasonable to assume that the delamination processes at both the molding compound and copper pad interface and silicon die and die attach interface can alter the stress distribution over the surface of the silicon die. Even after the stress transformation into one single value per cell and cycle, it is still difficult to analyze the data in the form of 480 cells, see Figure 7. A certain load metric, which well represents the effect of CTE mismatch and integrates data from the 480 cells, is required to represent the applied loading [22].

A load metric can be defined using the stress signals from all 480 cells as:

$$\sigma^* = \frac{\sum_{i=1}^{480} |D(\sigma)_i|}{480} \tag{3}$$

In this manner, the data from 480 parameters was reduced to a single value, which makes analyzing the stress feasible. Using this procedure, the stress response for the whole die can be visualized, as depicted in Figure 8. Sudden increases or sudden drops in stress indicates delamination initiation and propagation in the package. It is important to recall that the crack propagation rate is inversely proportional to the rate of the interface stiffness change, i.e., the stress rate changes with the crack propagation rate.

Visualizing the data from the TV $MC1\_1$ on Figure 8, the following observations are made:

- Between 0 and 750 TS cycles, the stresses have a relatively constant value. Small changes are observed due to the moisture release and relaxation effects. This can be also attributed to the effect of aging-induced oxidization on the package stress that has been reported recently [23].
- Around a TS cycle of 850, there is a small drop followed by a large sudden increase of the stress, indicating a significant change in the package structure.
- Afterwards, the stresses change at a slow rate, but still follow the same trend of increasing for approximately additional 500 cycles until reaching the maximum value. This indicates further changes in the structure.
- From 1350 TC cycle onwards, the stresses increase initially at a fast rate but the rate becomes slow. This is an indication that the changes inside the package reach the ending phase.

The overall behavior of the stresses in $MC1\_2$ TV is constant during the TS, indicating no changes in the package structure. In comparison with the $MC1\_1$ the stress behavior does not show any initial changes linked to the moisture and also no sudden drops. There are only few small changes, caused by interruption of the experiment. The visualization metric of all samples are depicted in Figure 8. Based on these initial plots, it is observed that all other samples $MC2\_1$, $MC2\_2$, $MC2\_3$ and $MC2\_4$ have some initial delamination. It is speculated that the interface toughness between the molding compound and the copper pad in case of $MC2$ is smaller than that in the case of $MC1$. The next subchapter explains how the changes shown by the visualization metric are connected to the delamination.

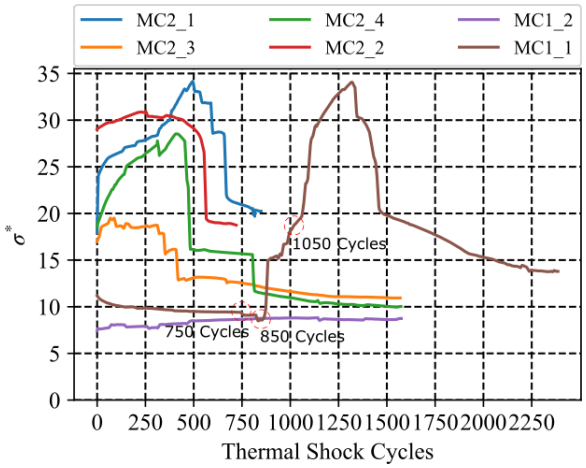

Fig. 8. Visualization Metric. The sum of absolute stress value change divided by the number of cells in cycle time for $MC1$ and $MC2$.

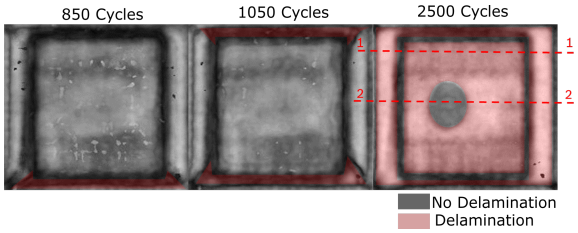

Fig. 9. SAM of $MC1\_1$ during and after the experiment. Delamination is detected and is depicted in red areas. Two cross-section are performed at the end of the experiment.

C. Failure Analysis

Using the visualization metric, a change in the sensor data was observed, indicating a shift from the normal conditions. These observations are confirmed by the physical failure and the location documented by scanning acoustic microscope images and cross-section images.

The relative stress difference was correlated with delamina-

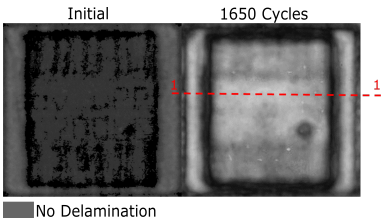

Fig. 10. SAM of $MC1\_2$ in discrete time. No delamination is present and one cross-section is performed at the end of the experiment.

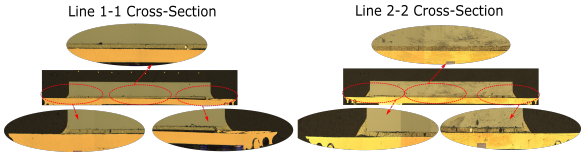

Fig. 11. Cross-section Failure Analysis of $MC1\_1$ along Line 1-1 and Line 2-2. Crack is present at the interface between molding compound/copperpad and die attach/copper pad along the entire cross-section for Line 1-1, except the middle part in Line 2-2.

tion using Scanning Acoustic Microscope (SAM) images. The SAM images taken at various stages are shown in Figure 9. The samples were taken out from the TS chamber for taking SAM images. The cables were removed for SAM imaging, and they were re-soldered to the samples before placing them back in the TS chambers. The state of the package $MC1\_1$ before and after 750 TS does not show any delamination (Figure 9). The significant change in the stress is observed around 850 Cycles. A SAM analysis was performed again at 850 cycles, and the image is shown in Figure 9. The image clearly shows that delamination started at the bottom of the package, which correlates well with the sudden increase in stress shown in Figure 8 for $MC1\_1$.

The same sample was tested again by SAM after additional 200 TS cycles. The image shows that a new delamination started on the other side while the first delamination propagated. The SAM image confirmed the crack growth. The stress history in Figure 8 (the maximum stress levels at that specific point in time) also corroborates this.

At the end of the Experiment, at around 2500 TS cycles, another SAM analysis was performed. The image clearly shows that delamination occurred everywhere except for a small area at the center (Figure 9). To further validate the correlation, a destructive failure analysis was performed after the TS cycling. The cross-section images along Line 1-1 of $MC1\_1$ are shown in Figure 11. The images show clearly cracks at all three interfaces (molding compound/copper pad, silicon die/die attach, and die attach/copper pad), which validates the SAM investigation. The cross-section images along Line 2-2 of $MC1\_1$ are shown in Figure 11. The images clearly indicate the presence of cracks at all three interfaces. The images also confirm the interface with no delamination that the SAM images were able to identify.

In the case of TV $MC1\_2$, there was no significant change in stresses during the experiment, indicating that no delamination occurred. This is confirmed by the SAM images obtained after the experiment (Figure 10). It was further corroborated by the cross-section images.

V. Diagnostics

Diagnostics consists of two steps: fault detection by Mahalanobis Distance (MD) and fault clarification by a clustering technique.

A. Fault Detection

Fault detection by MD was described in details for fault classification in [8] and for fault detection in [10] [24]. Mahalonobis distance is the distance between a point and a distribution. And not between two distinct points, like Euclidean distance. It is effectively a multivariate equivalent of the Euclidean distance. Basically, is the normalized distance between the test point from the sample mean over the standard deviation. A healthy baseline and a threshold are needed to classify the product states (healthy or unhealthy). They are determined by the well-known Mahalanobis Distance (MD). The methodology begins with gathering the sensor data, i.e., the values of stress difference at the 480 sensor cells. These values are referred to as performance parameters. They are stored in a matrix X_{ij} with elements denoted as xij, where $i = 1, 2, ..., p$ and p is the total number of performance parameters (here $p = 480$) and $j = 1, 2, ..., m$ where m is the total number of measurement points. A representative MD applied to the stress sensor cells is shown in Figure 12. The healthy baseline is created on the first 800 measurement points of no delamination. The data points exceeding the failure limit are clearly seen in the MD results after 850 Cycles, where delamination occurred. The failure detection point is defined. The threshold was computed from the healthy data (i.e., no initial delamination). The result is also plotted in Figure 12.

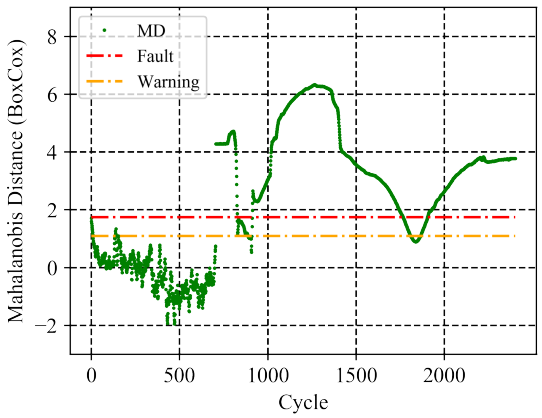

Fig. 12. Classic threshold MD applied to TQFP stress sensor data. The fault is detected around 850 Cycles.

Since the MD are not normally distributed, a Box-Cox transformation [25] is used to convert the data into a normal distribution. A warning limit threshold is defined as $(\mu + 2\sigma)$ and a fault alarm threshold as $(\mu + 3\sigma)$, based on the normal distribution parameters. A limitation of the Mahalanobis distance is found that the healthy baseline cannot be updated.

B. Fault Classification

One way of classifying the data is $clustering$, which is a common unsupervised ML technique. Its aim is to divide objects into groups according to distance-based similarity measure [26]. This method is chosen because of its computational effectiveness amongst other unsupervised ML methods. A clustering technique is used to classify the data. To reveal hidden information such as the necessary number of clusters, the Elbow method, described in [26], is used. All the 480 stress sensing cells are used in the algorithm. Based on the elbow method, only three clusters are needed to correctly split the data. Based on the number of prediction class output and the previous knowledge from failure analysis, three subgroups are identified. This can be visualized in Figure 13, as follows: the first subgroup is the healthy class 2 until 880 TS cycle; the second subgroup is the data associated with the delaminated copper pad/molding compound interface; and the third subgroup contains the data obtained after 1450 cycles onwards attributed to the delamination at the adhesive/silicon die interface.

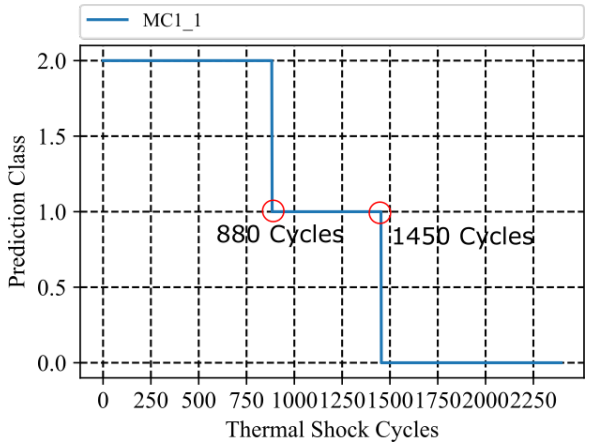

Fig. 13. Prediction Class with K-Means Clustering method. 2 - represents the health state; 1 - the delamination between molding compound and copper pad; 0 - delamination between the adhesive and silicon die.

TABLE II
CONTOUR PLOT STANDARD DEVIATION.

Input: Stress Difference $D(\sigma)_{ijk}$, Cycle Interval
Output: Standard Deviation SD_{ijl} per Interval
Step 1. Calculate the average of each column: $\bar{x_{ij}} = \frac{1}{r}\sum_{l=1}^{r} D(\sigma)_{ij}$
Step 2. Calculate the standard deviation: $SD_{ij} = \sqrt{\frac{\sum_{l=1}^{r}(D(\sigma)_{ij} - \bar{x_{ij}})^2}{r-1}}$
Step 3. Plot the contour matrix SD_{20x24}.
Step 4. Evaluate the crack tip on the contour plot.
$*i = 1, 2, ..., n$ and $n = 20$ number of cells in x direction
$*j = 1, 2, ..., m$ and $m = 24$ number of cells in y direction
$*k = 1, 2, ..., p$ and $p =$ number of cycles
$*l = 2, ..., r$ and $r =$ Cycle Interval where standard deviation is calculated

The results from the clustering are an indirect validation of the assumption in the section IV that delamination starts at the outer areas of the silicon die, resulting in an increase in the stress difference.

C. Fault Location

As depicted in Figure 3 the silicon die consists of 20 sensing cells on x direction and 24 cells on y, respectively. It is observed that high value of the Standard Deviation (SD) per each r number of interval cycles, corresponds to the crack tip location in the adhesive layer. The steps followed in calculation of the SD is described in Table II.

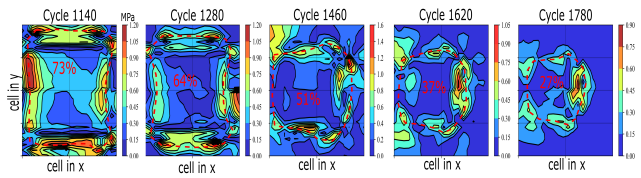

Fig. 14. Stress Difference SD every 20 Cycles plotted on a contour image for $MC1\_1$. The crack tip is given by the high SD.

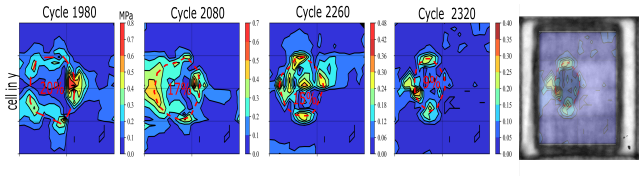

Fig. 15. Stress Difference SD every 20 Cycles plotted on a contour image for $MC1\_1$. The crack tip is given by the high standard deviation. This is validated over the SAM images on this TV, but also on the other TVs.

For this case an interval of 20 cycles is chosen to evaluate the standard deviation. This value is chosen to have an effective number of pictures that needs to be manually evaluated. Some of them are depicted in Figure 14 and 15. It is clearly shown that the high values of standard deviation in the contour plot corresponds to the crack tip in the adhesive layer. This way it is possible to follow the crack tip delamination area at least every 2 cycles.

In Figure 15 an SD contour plot image is overlaid over the SAM image. This corroborates with our observation that the high values of SD indicates the location of the crack tip. This validation is performed on all the other SAM images available and validates our observations.

Every image is then manually evaluated and a red dotted path is drawn over the high values of the SD. The area formed inside the path is then divided by the total area of the sensor area and transformed into percentage. Therefore, at least every 2 cycles an estimated remaining not delaminated area can be manually evaluated.

VI. HEALTH ASSESSMENT AND PROGNOSTICS

A. Degradation estimation

ESN is a new type of Recurrent Neural Network (RNN) proposed in recent years, and was developed by Jaeger [27]. The training process of ESN is easier and less computationally intensive than regular RNN which has the same size [28].

Remaining useful life (RUL) is the amount of time left before a system fails to operate within acceptable limits. RUL calculation is similar to Time-to-Failure (TTF) calculation, except that an upper operating limit threshold is used instead of a failure threshold [29]. Defining a degradation threshold for RUL is a challenging task as it strictly depends on applications. Various application-specific integrated circuits (ASICs) can be packaged in the same type of the housing, such as TQFP. For an application with relatively small power dissipation (below 1 W), only 10% of the die attach contact area can still provide good functionality of the ASIC, while for other application with larger power dissipation, even 20% of the contact area can bring the device to an end of life. In our study, we have assumed that 10% of the contact area as a threshold for an end of life, i.e., a good connection between silicon die and die paddle is assumed to be provided even after 90% of the die attach is delaminated. It is to be noted that the threshold value should be adjusted for different applications. In this paper, the ESN method is used for the estimation and prediction of degradation based on incremental stress values. The RUL is

predicted by extrapolation from the degradation estimation. For the purpose RUL calculation, the degradation grades of "complete delamination" and "no delamination" are set to be 0% and 100%, respectively. Half of the TVs data $MC1\_1$, $M2\_1$ and $M2\_4$ is used for both training set and testing set. The data from $M1\_2$, ,$M2\_2$ and $M2\_3$ are used for the analysis. In a real time prognosis, the inputs are the stress difference of that specific point in time, and the output will be the degradation estimation percentage. The input of ESN is defined as all relative stresses $D(\sigma)$ of all valid measurement points in all sensors as:

$$u = D(\sigma)_{ij} \tag{4}$$

,where $i = 1, 2, ..., n$ and $n =$ total number of cells (480 in this case) and $j = 1, 2, ..., m$ and $m =$ number of cycles.

Output of ESN defined as the degradation grade is a function, from 100% to 0% created based on the SD values. This evaluation is perfomed manually on the contour plot image every 20 cycles. This is a time consuming task and therefore needs to be automated. Traning half of the TVs data is an attempt to generalize the model. The rest of TVs data is evaluated by the model, without being neccessary to manually evaluate the delamination area based on the fault location.

$$y = \begin{pmatrix} 100\% \\ \frac{R_1}{N} \times 100\% \\ \frac{R_2}{N} \times 100\% \\ \vdots \\ \frac{R_n}{N} \times 100\% \\ 0\% \end{pmatrix} \tag{5}$$

,where R is the area evaluated by manually drawing a red dotted path and N is the total area of the physical sensor.

Data from three TVs $MC1\_1$, $M2\_1$ and $M2\_4$ were used to train the network. Cross-validation was used in the training process that involved the separation of data into k folds. In this study $k = 10$ was used. After the division, the model was trained on 9 of these folds and then was subsequently validated using the remaining fold. The average of the 10 measures mean square error (MSE) was the metric used to improve the model.

Up to the point where there is a failure detected the output is considered 100% as of no delamination is present. Afterwards, a manually created function is used to describe the degradation (equation 5).

The parameter size of dynamic reservoir n, the desired spectral radius of dynamic reservoir r, the input shift and scaling, and the output shift and scaling have to be optimized. The commonly used range of parameters are shown in Table III.

The optimization strategy used in this case is a conservative one. Changing one parameter with a certain step, keep others unchanged, train the ESN using the cross-validation to get the lowest MSE.

During optimization, the ESN was trained and tested for 10^6 times. The minimum MSE was then found, and its combination of parameter was recorded. The optimization process took about 5 hours. From this optimization, it is

TABLE III
RANGE OF PARAMETERS OF RNN [30].

Parameter	Commonly used range
Reservoir size	[50,800]
Spectral radius	[0.1,1)
Input scaling	[0,1]
Input shift	$[0, \max_{input}]$
Output scaling	[0,1]
Output shift	$[0, \max_{output}]$

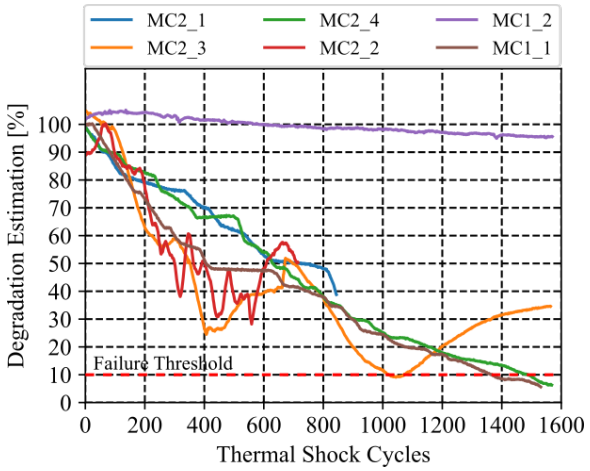

Fig. 16. Degradation estimation ESN Output for $MC1$ and $MC2$.

observed that the reservoir size and the spectral radius are two main factors influencing MSE. A very good practical guideline can be found in [31]. The execution time of the model is $659ms$ for fitting and $745ms$ for prediction, on a regular office Degradation prediction in percentage for all the testing modules are shown in Figure 16. Degradation percentages here refer to delamination area. Comparing the results from the ESN prediction and the SAM images from Figure 17 the following can be stated:

- For TV $MC2\_1$ and $MC2\_2$ a 30% delamination area remaining is predicted by the ESN. This is validated by the SAM images.
- For TV $MC2\_3$ and $MC2\_4$ the model predicts an almost full delamination percentage close to few percentages. This is also confirmed by the SAM images.
- As expected for TV $MC1\_2$ no degradation is predicted.

Following the same methodology from the fault location section, the degradation estimation for the other TVs was also evaluated and is depicted in Figure 18. A comparison between

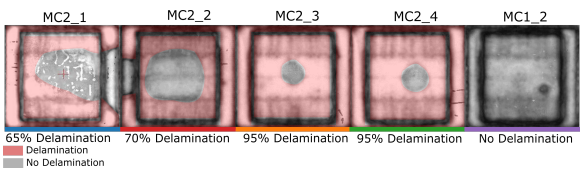

Fig. 17. SAM Images at the end of the experiments for $MC1$ and $MC2$.

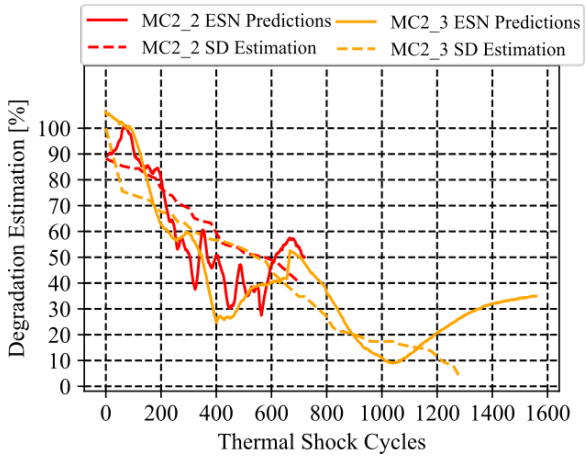

Fig. 18. Degradation estimation ESN Output vs SD Estimation.

the ESN model and SD methodology is shown. The results shows good accuracy in generalization of ESN model. The model can be, of course, improved by including more samples data into the training data.

Based on the neural network model, RUL estimation can be extrapolated. However, how to extrapolate RUL from this model under real operating conditions still remains a challenge that must be addressed in the future studies. It is observed that the RUL for all the modules strongly depends on the failure detection point, the loading conditions and material properties.

VII. Conclusion

The thermo-mechanical stress-based prognostics approach was developed to extend the stress-based PHM capability into a quantitative domain where accurate prediction of remaining useful life (RUL) became possible. The approach was implemented with actual microelectronics packages subjected to harsh accelerated testing conditions. Piezoresistive stress sensors were employed to measure the internal stresses of microelectronic packages. An Acquisition Unit (AU) and a Raspberry Pi were used for sensor data read-out, collection and evaluation. Accelerated tests in a thermal convection chamber were performed, and the resultant failure data were utilized to conduct data processing. The statistical techniques for diagnostics and the machine learning (ML) algorithms for health assessment and prognostics were then implemented to estimate and predict the degradation state.

The neural network model used in the paper was built and tested by using one half of TVs as a training set and the other half of TVs as a testing set. The network parameters were optimized only for these datasets. More data sets must be obtained to train and test the network so that a more generalized model can be created. Nevertheless, the results show that the proposed framework and approach outperforms the conventional failure analysis approach (e.g., SAM analysis). The results also confirm that data driven approaches provide the opportunity not only to monitor the asset during operation, but also to understand the asset behavior based on its current design. This can lead to a better product in the future and to further optimize resources and expenditures.

Acknowledgment

The work was funded by the Federal Government of Germany, Framework Program for Research and Innovation 2016-2020 Microelectronics - Innovation Drivers of Digitalization (Rahmenprogramm der Bundesregierung für Forschung und Innovation 2016-2020 Mikroelektronik aus Deutschland - Innovationstreiber der Digitalisierung) - Project smartSTAR (No. 16ES0965). This funding is gratefully appreciated.

References

[1] W.-S. Lei and A. Kumar, "Delamination and reliability issues in packaged devices," in *Adhesion in Microelectronics*, K. Mittal and T. Ahsan, Eds., pp. 267–312. John Wiley & Sons, Inc., 2014. [Online]. Available: http://doi.wiley.com/10.1002/9781118831373.ch7

[2] G. Q. Zhang, W. D. v. Driel, and X. J. Fan, *Mechanics of microelectronics*, ser. Solid mechanics and its applications, no. v. 141. Springer, 2006, OCLC: ocm70268148.

[3] N. Vichare and M. Pecht, "Prognostics and health management of electronics," *IEEE Transactions on Components and Packaging Technologies*, vol. 29, DOI 10.1109/TCAPT.2006.870387, no. 1, pp. 222–229, 2006. [Online]. Available: http://ieeexplore.ieee.org/document/1599514/

[4] Y. Zou, J. C. Suhling, R. W. Johnson, and R. C. Jaeger, "Complete stress state measurements in chip on board packages," in *Multichip Modules and High Density Packaging, 1998. Proceedings. 1998 International Conference on*, pp. 405–415. IEEE, 1998. [Online]. Available: http://ieeexplore.ieee.org/abstract/document/670816/

[5] A. R. R. Adli, K. M. B. Jansen, F. Schindler-Saefkow, and F. Rost, "Experimental investigation and interpretation of the real time, in situ stress measurement during transfer molding using the piezoresistive stress chips," in *Thermal, mechanical and multi-physics simulation and experiments in microelectronics and microsystems (eurosime), 2014 15th international conference on*, pp. 1–4. IEEE, 2014. [Online]. Available: http://ieeexplore.ieee.org/abstract/document/6813837/

[6] Y. Zou, J. C. Suhling, R. W. Johnson, R. C. Jaeger, and A. K. M. Mian, "In-situ stress state measurements during chip-on-board assembly," *IEEE Transactions on Electronics Packaging Manufacturing*, vol. 22, no. 1, pp. 38–52, 1999. [Online]. Available: http://ieeexplore.ieee.org/abstract/document/755088/

[7] A. Palczynska, P. J. Gromala, D. Mayer, B. Han, and T. Melz, "In-situ investigation of EMC relaxation behavior using piezoresistive stress sensor," *Microelectronics Reliability*, vol. 62, pp. 58–62, 2016. [Online]. Available: http://www.sciencedirect.com/science/article/pii/S0026271416300488

[8] A. Prisacaru, A. Palczynska, A. Theissler, P. Gromala, B. Han, and G. Q. Zhang, "$in\ situ$ failure detection of electronic control units using piezoresistive stress sensor," *IEEE Transactions on Components, Packaging and Manufacturing Technology*, vol. 8, DOI 10.1109/TCPMT.2018.2816259, no. 5, pp. 750–763, 2018-05. [Online]. Available: https://ieeexplore.ieee.org/document/8331950/

[9] B. Wu, D.-S. Kim, B. Han, A. Palczynska, A. Prisacaru, and P. J. Gromala, "Hybrid approach to conduct failure prognostics of automotive electronic control unit using stress sensor as in situ load counter," *IEEE Transactions on Components, Packaging and Manufacturing Technology*, DOI 10.1109/TCPMT.2018.2815633, pp. 1–11, 2018. [Online]. Available: http://ieeexplore.ieee.org/document/8331923/

[10] A. Palczynska, A. Prisacaru, P. J. Gromala, B. Han, D. Mayer, and T. Melz, "Towards prognostics and health monitoring: The potential of fault detection by piezoresistive silicon stress sensor," in *Thermal, Mechanical and Multi-Physics Simulation and Experiments in Microelectronics and Microsystems (EuroSimE), 2016 17th International Conference on*, pp. 1–8. IEEE, 2016. [Online]. Available: http://ieeexplore.ieee.org/abstract/document/7463344/

[11] A. Prisacaru, A. Palczynska, P. J. Gromala, B. Han, and G. Q. Zhang, "Condition monitoring algorithm for piezoresistive silicon-based stress sensor data obtained from electronic control units," DOI 10.1109/ECTC.2017.73, pp. 1119–1127. IEEE, 2017-05. [Online]. Available: http://ieeexplore.ieee.org/document/7999824/

[12] F. Schindler-Saefkow, F. Rost, A. Otto, W. Faust, B. Wunderle, B. Michel, and S. Rzepka, "Stress chip measurements of the internal package stress for process characterization and health monitoring," in *2012 13th International Thermal, Mechanical and Multi-Physics*

Simulation and Experiments in Microelectronics and Microsystems, DOI 10.1109/ESimE.2012.6191746, pp. 1/10–10/10, 2012.

[13] M. K. Rahim, J. C. Suhling, R. C. Jaeger, and P. Lall, "Fundamentals of delamination initiation and growth in flip chip assemblies," in *Proceedings Electronic Components and Technology, 2005. ECTC '05.*, DOI 10.1109/ECTC.2005.1441420, pp. 1172–1186 Vol. 2, 2005.

[14] A. Prisacaru, E. O. Guerrero, P. J. Gromala, B. Han, and G. Q. Zhang, "Degradation prediction of electronic packages using machine learning," in *2019 20th International Conference on Thermal, Mechanical and Multi-Physics Simulation and Experiments in Microelectronics and Microsystems (EuroSimE)*, DOI 10.1109/EuroSimE.2019.8724523, pp. 1–9, 2019.

[15] A. Prisacaru, A. Palczynska, P. Gromala, B. Wu, B. Han, and G. Zhang, "Accuracy of cmos-based piezoresistive stress sensor for engineering applications of thermal loading condition: Theoretical review and experimental validation," *IEEE Sensors Journal*, vol. 19, no. 20, pp. 9139–9148, 2019.

[16] R. Jaeger, J. Suhling, R. Ramani, A. Bradley, and Jianping Xu, "CMOS stress sensors on [100] silicon," *IEEE Journal of Solid-State Circuits*, vol. 35, DOI 10.1109/4.818923, no. 1, pp. 85–95, 2000-01. [Online]. Available: http://ieeexplore.ieee.org/document/818923/

[17] R. B. GmbH, "Abschlussbericht zum verbundvorhaben iforcesens: Entwicklung eines integrierten stressmesssystems zur quantifizierung der 3 d-v erformung von sensorbauelementen in abhangigkeit des verpackungsprozesses," *Technische Informationsbibliothek*, DOI https://doi.org/10.2314/GBV:606643435, 2008. [Online]. Available: https://doi.org/10.2314/GBV:606643435

[18] H. Kittel, S. Endler, H. Osterwinter, S. Oesterle, and F. Schindler-Saefkow, "Novel stress measurement system for evaluation of package induced stress," in *Integration Issues of Miniaturized Systems-MOMS, MOEMS, ICS and Electronic Components (SSI), 2008 2nd European Conference & Exhibition on*, pp. 1–8. VDE, 2008. [Online]. Available: http://ieeexplore.ieee.org/abstract/document/5760504/

[19] A. Palczynska, F. Pesth, P. J. Gromala, T. Melz, and D. Mayer, "Acquisition unit for in-situ stress measurements in smart electronic systems," in *Thermal, mechanical and multi-physics simulation and experiments in microelectronics and microsystems (eurosime), 2014 15th international conference on*, pp. 1–4. IEEE, 2014. [Online]. Available: http://ieeexplore.ieee.org/abstract/document/6813795/

[20] S. Naduvil-Vadukootu, R. Angryk, and P. Riley, "Evaluating preprocessing strategies for time series prediction using deep learning architectures," 2017. [Online]. Available: https://aaai.org/ocs/index.php/FLAIRS/FLAIRS17/paper/view/15475

[21] S. A. Alasadi and W. S. Bhaya, "Review of data preprocessing techniques in data mining," *Journal of Engineering and Applied Sciences*, vol. 12, DOI http://dx.doi.org/10.3923/jeasci.2017.4102.4107, no. 16, pp. 4102 – 4107, 2017. [Online]. Available: http://medwelljournals.com/abstract/?doi=jeasci.2017.4102.4107

[22] Y.-H. Yang, B. Han, A. Prisacaru, P. Gromala, S. Jiang, and A. Sarwar, "In-situ service load monitoring of automotive electronic systems using silicon-based piezoresistive stress sensor," *Microelectronics Reliability*, vol. 110, DOI 10.1016/j.microrel.2020.113650, p. 113650, 07 2020.

[23] A. Inamdar, A. Prisacaru, M. Fleischman, E. Franieck, P. Gromala, A. Veres, C. Nemeth, Y. Yang, and B. Han, "Study of thermal aging behavior of epoxy molding compound for applications in harsh environments," in *2019 IEEE 69th Electronic Components and Technology Conference (ECTC)*, pp. 811–818, 2019.

[24] S. Kumar, T. Chow, and M. Pecht, "Approach to fault identification for electronic products using mahalanobis distance," *IEEE Trans. Instrum. Meas.*, vol. 59, DOI 10.1109/TIM.2009.2032884, pp. 2055 – 2064, 09 2010.

[25] M. Pecht, "Prognostics and health monitoring of electronics," in *Electronic Materials and Packaging, 2006. EMAP 2006. International Conference on*, pp. 1–10. IEEE. [Online]. Available: http://ieeexplore.ieee.org/xpls/abs_all.jsp?arnumber=4430561

[26] F. Pedregosa, G. Varoquaux, A. Gramfort, V. Michel, B. Thirion, O. Grisel, M. Blondel, P. Prettenhofer, R. Weiss, V. Dubourg, J. Vanderplas, A. Passos, D. Cournapeau, M. Brucher, M. Perrot, and E. Duchesnay, "Scikit-learn: Machine learning in Python," *Journal of Machine Learning Research*, vol. 12, pp. 2825–2830, 2011.

[27] H. Jaeger, "Harnessing nonlinearity: Predicting chaotic systems and saving energy in wireless communication," *Science*, vol. 304, DOI 10.1126/science.1091277, no. 5667, pp. 78–80, Apr. 2004. [Online]. Available: https://doi.org/10.1126%2Fscience.1091277

[28] J. Dai, G. K. Venayagamoorthy, and R. G. Harley, "An introduction to the echo state network and its applications in power system," in *2009 15th International Conference on Intelligent System Applications to Power Systems*, DOI 10.1109/ISAP.2009.5352913, pp. 1–7, Nov. 2009.

[29] D. Galar, U. Kumar, J. Lee, and W. Zhao, "Remaining useful life estimation using time trajectory tracking and support vector machines," *Journal of Physics: Conference Series*, vol. 364, DOI 10.1088/1742-6596/364/1/012063, p. 012063, May. 2012. [Online]. Available: https://doi.org/10.1088%2F1742-6596%2F364%2F1%2F012063

[30] E. Z. Marco Rigamonti, Piero Baraldi, *Echo State Network for the Remaining Useful Life Prediction of a Turbofan Engine*. European Conference of the Prognostics and Health Management Society, 2016.

[31] M. Lukosevicius, *A Practical Guide to Applying Echo State Networks*. Springer, 2012.

Alexandru Prisacaru is currently a PhD candidate located at Bosch, Automotive Electronics in Reutlingen. His PhD work is performed in cooperation with Delft University of Technology "Micro/Nanoelectronics System Integration and Reliability" department. His research activities focus on developing and implementing Prognostics and Health Management techniques of relevant electronics for future autonomous driving applications. Amongst these his technical expertise include computational structural mechanics, material modeling, statistical pattern recognition, machine learning methods and surrogate modeling. He holds a Master degree in Computational Engineering from Ruhr University of Bochum, Germany and a Master degree in Structural Engineering from Technical University "Gheorghe Asachi" Iasi, Romania.

Przemyslaw Gromala is a simulation senior expert at Robert Bosch GmbH, Automotive Electronics in Reutlingen. Currently leading an international simulation team and FEM verification lab with the main focus on implementation of simulation driven design for electronic control modules and multi-chip power packaging for hybrid drives. His research activities focus on virtual pre-qualification techniques for development of the electronic control modules and multi-chip power packaging. His technical expertise includes material characterization and modeling, multi-domain and multi-scale simulation incl. fracture mechanics, verification techniques and prognostics and health monitoring for future safety related electronic smart systems. Prior joining Bosch Mr Gromala worked at Delphi development center in Krakow, as well as at Infineon research and development center in Dresden. He is an active committee member of the IEEE conferences: ECTC, EuroSimE, ICEPT; ASME: InterPACK. Active committee member of EPoSS ? defining R&D and innovation needs as well as policy requirements related to Smart Systems Integration and integrated Micro- and Nanosystems. He holds a PhD in mechanical engineering from Cracow University of Technology in Poland.

Bongtae Han received his BS and MS degrees in Mineral and Petroleum Engineering from Seoul National University in 1981 and 1983, respectively, and his Ph.D. degree in Engineering Mechanics from Virginia Tech in 1991. Dr. Bongtae Han is Keystone Professor of Engineering and APT Chair of the Mechanical Engineering Department of the University of Maryland; and is currently directing the LOMSS (Laboratory for Optomechanics and Micro/nano Semiconductor/Photonics Systems) of CALCE (Center for Advanced Life Cycle Engineering). Dr. Han has co-authored a text book entitled "High Sensitivity Moiré: Experimental Analysis for Mechanics and Materials", Springer-Verlag (1997) and edited two books. He has published 12 book chapters and over 250 journal and conference papers in the field of microelectronics, photonics and experimental mechanics. He holds 2 US patents and 4 invention disclosures. Dr. Han received the IBM Excellence Award for Outstanding Technical Achievements in 1994. He was a recipient of the 2002 Society for Experimental Mechanics (SEM) Brewer Award for his contributions to development of photomechanics tools used in semiconductor packaging. Most recently, he was named the 2016 American Society of Mechanical Engineering (ASME) Mechanics Award winner in Electronic and Photonic Packaging Division for his contributions to structural mechanics of electronic systems. His publication awards include (1) the Year 2004 Best Paper Award of the IEEE Transactions on Components and Packaging Technologies, (2) the Gold Award (best paper in the Analysis and Simulation session) of the 1st Samsung Technical Conference in 2004 and (3) the Year 2015 Best Paper Award of the 16th International Conference on Electronic Packaging Technology (ICEPT 2015). He served as an Associate Technical Editor for Experimental Mechanics, from 1999 to 2001, and Journal of Electronic Packaging, Transaction of the ASME from 2003 to 2012. He is currently serving as an Associate Editor for Microelectronics Reliability. He was elected a Fellow of the SEM and the ASME in 2006 and 2007, respectively.

Guo Qi Zhang is a IEEE Fellow, chair professor for "Micro/Nanoelectronics System Integration and Reliability" of Delft University of Technology. He authored/co-authored more than 350 scientific publications; chaired /co-chaired several international conferences; serves as associated editor for 3 international journals and chief editor for Springer book series "SSL Technology and Applications". He serves as deputy director of European Center for Micro- and Nanoreliability (EUCEMAN); co-chair of Advisory Board of International Solid State Lighting Alliance (ISA); secretary general of ITRW (International Technology Roadmap of Wide band gap semiconductors). He chaired the Eniac Strategic Research Agenda team of More than Moore; served as co-chair of academic council of Dutch national innovation program on Micro/nanoelectronics and embedded system. Prof. Zhang has also worked for NXP Semiconductors as Senior Director of Technology Strategy, Philips Research Fellow until May 2013.